

# Advanced Image Processing Techniques for the Discrimination of Buried Objects

Rodolfo Araneo<sup>1</sup> and Sami Barmada<sup>2</sup>

<sup>1</sup>Department of Electrical Engineering  
Sapienza University of Rome, Rome, 00184, Italy  
rodolfo.araneo@uniroma1.it

<sup>2</sup>Department of Energy and Systems Engineering  
University of Pisa, Pisa, 56122, Italy  
sami.barmada@dsea.unipi.it

**Abstract** — A numerical study for the electromagnetic detection of buried objects is presented. The whole GPR set-up is simulated through an integral formulation solved by means of the Method of Moments and a new discrimination process based on the 2D-Wavelet decomposition of computed electric field maps is proposed. The new wavelet methodology proves to be an effective tool for discrimination even in presence of noise.

**Index Terms** — 2D wavelet decomposition, GPR, MoM.

## I. INTRODUCTION

Electromagnetic induction sensors (EMIS) and ground penetrating radars (GPR) are tools commonly used to find buried objects, such as antipersonnel landmines (APM) [1-3]. The basic concept they are based on is to illuminate the target with an incident field (low-frequency magnetic or high-frequency electric field) and measure the broadband spectrum of the scattered field. Different sources, antennas, and sensors have been proposed in the past, such as horns, spirals, loaded-dipoles, or dielectric rods, loops [1-7].

The main issue is not the simple detection but the recognition of unknown buried objects, allowing to classify them as potential known targets or to discard them as clutters [1,2]. The recognition process necessarily needs the accurate design of the source system, detection sensors, and the development of post-processing algorithms

[7,8]. Moreover it is worth noting that the recognition problem becomes deeply more difficult in the presence of plastic landmines, when reflections greatly surpass and hide the weak field scattered by the buried plastic targets.

In this work, the behavior of a new high frequency system for the detection of buried objects is numerically investigated by an integral approach in conjunction with a method of moments (MoM) numerical tool. The key feature of the system lies in the fact that both the magnitude and phase of all the components of the scattered electric field are used to collect information about the EM behavior of the buried object [9]. Furthermore, the potentiality of a two dimensional post processing of the collected data based on a wavelet decomposition approach is investigated. The purpose is to highlight the features of the two-dimensional signature of the buried object significantly, facilitating its discrimination.

The MoM code proves to be a suitable and efficient tool for the study of these configurations, allowing a sensitivity analysis on the influence of material and shape variations.

In order to assess the robustness of the proposed technique, a Gaussian white noise has been added to the collected data before post processing. By adding the noise we try to simulate the uncertainties and the so called "physical noise" normally encountered in practical measurements; even in this case, the signature detection is satisfactory.

## II. EXPOSURE SET-UP

The set-up configuration is shown in Fig. 1. It consists of a double-ridged antenna which is used as a field source and an observation plane where the total field (incident plus scattered) is observed.

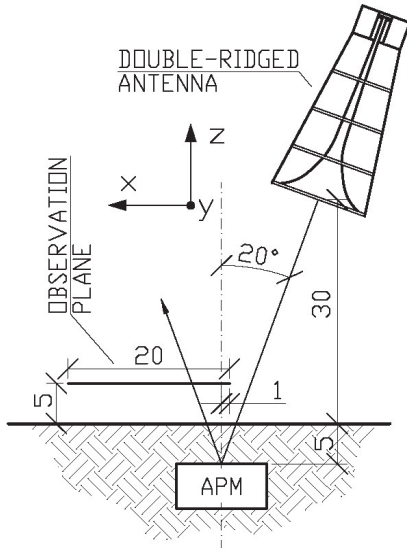


Fig. 1. Set-up configuration with a buried APM (units in cm).

The performances of the GPR are mainly affected by two key-points that must be accounted for in the optimization of the set-up.

The working frequency range must be a trade-off between penetration and resolution [2,5]. The direction and intensity of the reflection which occurs at the ground surface (ground bounce) depends on the electrical properties of the ground itself and the roughness of the surface while the penetration depth of the transmitted wave into the soil mainly depends on the ground humidity and the wavelength of the field. Lowering the working frequency of the GPR reduces the ground bounce and increases the penetration depth, but on the other side, it causes a loss of resolution in the received maps, which is necessary for an accurate detection of the buried object.

The height of the transmitting antenna must be a trade-off between transmitting antenna performance and enhancement of the received data [2,5]. A transmitting antenna closer to the ground surface shows better energy coupling with the target and reduced ground bounce, but the strong antenna-ground interaction can significantly change the antenna radiation properties, leading to

a large number of false alarms. Anyway, if elevating the transmitting antenna reduces the antenna interaction with the target and the ground, on the other hand, due to the roughness of the ground surface, it makes the observation plane receive the field scattered by a larger portion of the ground, leading to a more difficult target detection. To reduce the superposition of the field scattered by the soil, the ground is usually illuminated with an oblique angle.

In light of these remarks, the set-up shown in Fig. 1 has been chosen. The double ridge antenna is the Electrometrics EM-6961 model, which shows efficient performance characteristics in the frequency range 1-6 GHz. It has been chosen since it constitutes a good tradeoff between penetration and resolution [2-8]. The antenna has been tilted  $20^\circ$  around the y-axis and has been oriented with his E-plane on the xz-plane, as shown in Fig. 1. The total electric field (i.e. electric field radiated by the antenna plus that scattered by the soil and the target), is computed on the observation plane showed in Fig. 1. As for the measurement procedure of this field, the photorefractive effect of thin ferroelectric films [10] can be used and is now under investigation.

## III. NUMERICAL MODELING

### A. Integral equations

The whole GPR configuration has been studied through a standard integral formulation. The set of equations which solve the problem can be derived through a customary application of the equivalence principle [11]. First an equivalent electric current density  $\mathbf{J}_a$  is introduced over the PEC surface  $S_a$  of the antenna which is excited with a delta-gap voltage source. Next, equivalent electric  $\mathbf{J}_s$  and magnetic  $\mathbf{M}_s$  current densities are introduced on the surface  $S_s$  of the buried scattering object, which is considered penetrable. The boundary conditions at the surfaces  $S_a$  and  $S_s$  dictate a set of integral equations that can be written as

$$\mathbf{u}_n \times [\mathbf{E}^{\text{inc}} + \mathbf{E}^a + \mathbf{E}^s] = 0 \quad \mathbf{r} \in S_a \quad (1a)$$

$$-\mathbf{u}_n \times \mathbf{E}^{\text{inc}} = \mathbf{u}_n \times [\mathbf{E}^a + \mathbf{E}^s + \mathbf{E}_d^s] \quad \mathbf{r} \in S_s \quad (1b)$$

$$-\mathbf{u}_n \times \mathbf{H}^{\text{inc}} = \mathbf{u}_n \times [\mathbf{H}^a + \mathbf{H}^s + \mathbf{H}_d^s] \quad \mathbf{r} \in S_s, \quad (1c)$$

where  $(\mathbf{E}^{\text{inc}}, \mathbf{H}^{\text{inc}})$  is the incident field,  $(\mathbf{E}^{\text{a}}, \mathbf{H}^{\text{a}})$  is the field scattered from the PEC antenna,  $(\mathbf{E}^{\text{s}}, \mathbf{H}^{\text{s}})$  and  $(\mathbf{E}_{\text{d}}^{\text{s}}, \mathbf{H}_{\text{d}}^{\text{s}})$  are, respectively, the field scattered by the currents  $(\mathbf{J}_{\text{s}}, \mathbf{M}_{\text{s}})$  outside and inside the homogeneous penetrable target [11,12],  $\mathbf{u}_n$  is the outward unit vector normal to the surface. Equations (1a-1c) can be cast into coupled integral equations by expressing all fields as superposition integrals (symbol  $\otimes$ ) between the sources and the relevant dyadic Green functions (GFs):

$$\mathbf{E}_0^{\text{inc}} + \underline{\mathbf{G}}_{00}^{\text{EJ}} \otimes \mathbf{J}_{\text{a}} + \underline{\mathbf{G}}_{0\text{g}}^{\text{EJ}} \otimes \mathbf{J}_{\text{s}} + \underline{\mathbf{G}}_{0\text{g}}^{\text{EM}} \otimes \mathbf{M}_{\text{s}} = 0 \quad \mathbf{r} \in S_{\text{a}} \quad (2\text{a})$$

$$\mathbf{E}_{\text{g}}^{\text{inc}} + \underline{\mathbf{G}}_{\text{g}0}^{\text{EJ}} \otimes \mathbf{J}_{\text{a}} + \underline{\mathbf{G}}_{\text{gg}}^{\text{EJ}} \otimes \mathbf{J}_{\text{s}} + \underline{\mathbf{G}}_{\text{gg}}^{\text{EM}} \otimes \mathbf{M}_{\text{s}} + \underline{\mathbf{G}}_{\text{d}}^{\text{EJ}} \otimes \mathbf{J}_{\text{s}} + \underline{\mathbf{G}}_{\text{d}}^{\text{EM}} \otimes \mathbf{M}_{\text{s}} = 0 \quad \mathbf{r} \in S_{\text{s}} \quad (2\text{b})$$

$$\mathbf{H}_{\text{g}}^{\text{inc}} + \underline{\mathbf{G}}_{\text{g}0}^{\text{HJ}} \otimes \mathbf{J}_{\text{a}} + \underline{\mathbf{G}}_{\text{gg}}^{\text{HJ}} \otimes \mathbf{J}_{\text{s}} + \underline{\mathbf{G}}_{\text{gg}}^{\text{HM}} \otimes \mathbf{M}_{\text{s}} + \underline{\mathbf{G}}_{\text{d}}^{\text{HJ}} \otimes \mathbf{J}_{\text{s}} + \underline{\mathbf{G}}_{\text{d}}^{\text{HM}} \otimes \mathbf{M}_{\text{s}} = 0 \quad \mathbf{r} \in S_{\text{s}} \quad (2\text{c})$$

where the cross product with  $\mathbf{u}_n$  is suppressed for the sake of simplicity. In eqs (2), the incident fields  $(\mathbf{E}_{\text{g}}^{\text{inc}}, \mathbf{H}_{\text{g}}^{\text{inc}})$  and  $\mathbf{E}_0^{\text{inc}}$  are, respectively, those inside the ground and in free space due to the voltage source of the antenna,  $\underline{\mathbf{G}}_{lm}^{\text{PQ}}(\mathbf{r}, \mathbf{r}')$  is the dyadic GF relating the P-type field at the observation point  $\mathbf{r}$  in the medium  $l$  with the Q-type current source at source point  $\mathbf{r}'$  in the medium  $m$ , and  $\underline{\mathbf{G}}_{\text{d}}^{\text{PQ}}(\mathbf{r}, \mathbf{r}')$  is the PQ-type GF in the homogeneous dielectric space (inside the penetrable target). Obviously, when the target is a PEC object,  $\mathbf{M}_{\text{s}} = 0$  and eq. (2c) is not necessary anymore.

## B. Solution of the integral equations

To efficiently solve the system of equations (2) by means of the MoM technique, it is better to recast it in a mixed potential form [11,12]. Anyway, since in a layered medium the scalar potentials of a point charges associated with horizontal and vertical current dipoles are in general different [13,14], it is necessary to modify either the scalar or the vector potential kernel. Choosing the so-called Formulation C in [13] leads to

$$\mathbf{E}(\mathbf{J}) = \underline{\mathbf{G}}_{lm}^{\text{EJ}} \otimes \mathbf{J} = -j\omega\mu_0 \underline{\mathbf{G}}_{lm}^{\text{A}} \otimes \mathbf{J} + \frac{1}{j\omega\epsilon_0} \nabla \left( K_{lm}^{\text{V}} \otimes \nabla' \cdot \mathbf{J} \right) + C_{lm}^{\text{V}} \mathbf{u}_z \otimes \mathbf{J} \quad (3\text{a})$$

$$\mathbf{E}(\mathbf{M}) = \underline{\mathbf{G}}_{lm}^{\text{EM}} \otimes \mathbf{M} \quad (3\text{b})$$

$$\mathbf{E}(\mathbf{J}) = \underline{\mathbf{G}}_{lm}^{\text{HJ}} \otimes \mathbf{J} \quad (3\text{c})$$

$$\mathbf{H}(\mathbf{M}) = \underline{\mathbf{G}}_{lm}^{\text{HM}} \otimes \mathbf{M} = -j\omega\epsilon_0 \underline{\mathbf{G}}_{lm}^{\text{F}} \otimes \mathbf{M} + \frac{1}{j\omega\mu_0} \nabla \left( K_{lm}^{\text{W}} \otimes \nabla' \cdot \mathbf{M} \right) + C_{lm}^{\text{W}} \mathbf{u}_z \otimes \mathbf{M} \quad (3\text{d})$$

where  $\underline{\mathbf{G}}_{lm}^{\text{A/F}}(\mathbf{r}, \mathbf{r}')$  are the magnetic/electric vector potential GFs,  $K_{lm}^{\text{V/W}}$  are the corresponding scalar potentials and  $C_{lm}^{\text{V/W}}$  are the so called correction factors [13,14]. All the expressions of the GFs can be obtained through a transmission line analogy in the transformed spectral domain as in [14].

A standard MoM procedure has been used to solve the integral equations system (2), once it has been cast in an MPIE form. In particular, the antenna and the target surfaces have been discretized through nonoverlapping triangles, and the unknown current densities have been expanded by a set of second-order subdomain basis functions, which provide a linear-normal/quadratic-tangent (LN/QT) representation of the vector quantities [15]. All encountered singular terms in the source integrals (proportional to  $1/R$ ) have been extracted and integrated analytically [16], while the remaining (source and testing) integrals have been computed by means of standard Gaussian formulas [17]. For an efficient computation of the Sommerfeld integrals necessary to transform the GFs from the spectral to the spatial domain, the weighted-averages method has been used [18].

## C. Discretization of the problem

The antenna mesh is shown in Fig. 2a. The antenna is constituted of two exponentially shaped ridges, two lower and upper flares placed parallel to the H-plane (plane  $xz$  of Figs. 2) and thin copper straps placed parallel to the E-plane (plane  $yz$  of Figs. 2) [19,20]. The radiated field can be considered meanly linearly polarized with the E-field parallel to the  $y$ -axis and the H-field aligned with the  $x$ -axis.

The surface three-dimensional model of the antenna was entirely constructed with a

commercial CAD program and discretized with a professional mesh generator. The model is constituted of 3976 triangle patches, whose maximum edge length was forced to be below  $\lambda/10$  at the frequency of 6 GHz. The coaxial type N input connector was not simulated as in [19], and the scheme was excited with a lumped delta-gap voltage source placed between the two ridges in the lower cavity.

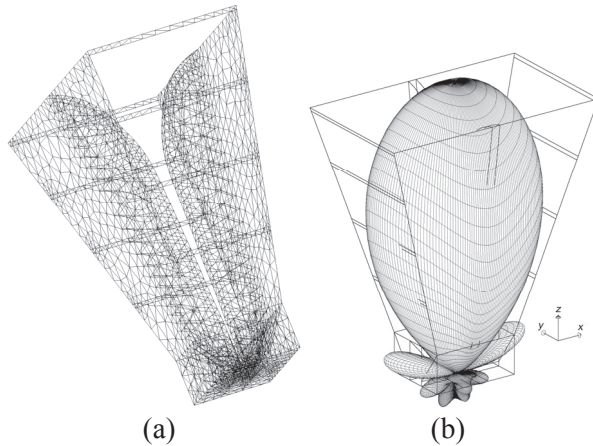


Fig. 2. Simulation model of the double-ridged antenna (a) and E-field radiation pattern (b).

The computed three dimensional pattern of the radiated E-field at 2 GHz, in the near field region ( $2D^2/\lambda = 52$  cm, with  $D$  maximum dimension of the radiating structure) at a distance of 50 cm, is shown in Fig. 2b, together with a magnification of the antenna (for the sake of clarity). Furthermore the electric field radiation patterns in the E- and H-planes are shown in Fig. 3. The 3dB beamwidth is around  $52^\circ$  and  $40^\circ$  in the E- and H- plane, respectively.

To test the effectiveness of the ground-penetrating system to distinguish between clutters and mines and to recognize the signature of a particular mine, the landmines and clutters shown in Fig. 4 have been considered [21]: the PMN ( $r=112$  mm,  $h=56$  mm) considered completely metallic, the PMA-1 ( $L=140$  mm,  $H=30$  mm,  $W=70$  mm) made of plastic with dielectric constant  $\epsilon_r = 4.8$ , a cylindrical clutter ( $r=10$  mm,  $L=100$  mm) and a spherical one ( $R=20$  mm), both considered perfectly conductive.

A realistic dielectric constant of 11.8 and loss tangent of 0.084 have been chosen for the ground in the frequency range of interest. The electric

field has been computed on the observation plane on a grid of  $64 \times 64$  points ( $2^6$ ), in order to allow the wavelet decomposition to the fifth level. The number of MoM unknowns is 2350; the CPU time and memory requirement for solving the described problem are, respectively, five minutes and 3 Gb on a four-core 3 GHz 64-bit desktop workstation.

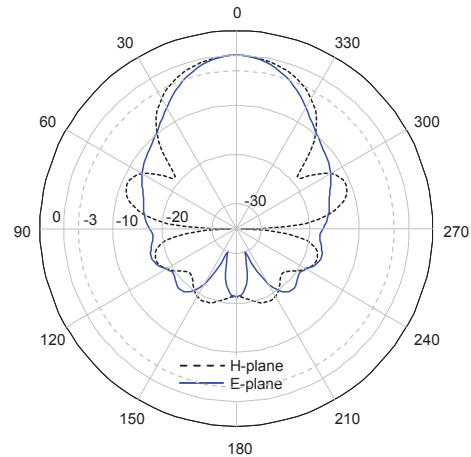


Fig. 3. E- and H- plane amplitude patterns of the double ridged antenna.

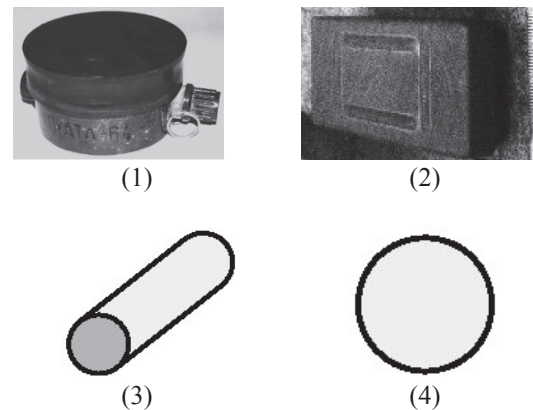


Fig. 4. Considered landmines – PMN (1) and PMA-1 (2) – and clutters – cylindrical (3) and spherical (4).

#### IV. IMAGE PROCESSING

As mentioned in the previous sections, both the magnitude and phase of all the components of the scattered electric field are used to collect information about the EM behavior of the buried object. This big amount of data can be easily represented by the use of two dimensional maps. The capability of the wavelet expansion tool in

signal processing is well established [22], and has been used also in electrical engineering in order to evidence special behavior of the analyzed quantities, which cannot be evidenced by a simple analysis of the signal in its unprocessed form [23, 24]. Furthermore, some attempts of wavelet based post processing in the area of discrimination of buried objects have been previously presented [25].

It is well-known that a multiresolution analysis is characterized by wavelet bases composed by the scaling functions  $\phi(x)$  and wavelet functions  $\psi(x)$ , the former being a low pass filter and the latter a high pass filter. A single dimension wavelet expansion yields a set of coefficients related to the correlation between a general function  $f(x)$  and the scaling and wavelet functions. In particular filtering performed by  $\phi(x)$  leads to what is called a “blurred version” of the original signal, while filtering with  $\psi(x)$  gives a signal containing the higher frequencies, called “detail”. Iteratively performing this sub band filtering (on the blurred version) leads to the multi – resolution decomposition of a signal in sum between a smooth signal (qualitatively an averaged signal) and a set of details.

In this case, we deal with 2D signals (the value of electric field on a plane) which can be easily organized in 2D color maps, i.e. figures to be analyzed by a proper technique.

The construction of two dimensional bases, necessary for image processing, is performed by using the so called separable wavelet bases, i.e. using the following basis functions

$$\begin{aligned}\phi^1(x, y) &= \phi(x)\phi(y) \\ \psi^1(x, y) &= \phi(x)\psi(y) \\ \psi^2(x, y) &= \psi(x)\phi(y) \\ \psi^3(x, y) &= \psi(x)\psi(y),\end{aligned}\tag{4}$$

in which functions at the same level of decomposition are used. Thinking about the frequency characteristics of the functions  $\phi(x)$  and  $\psi(x)$ , it is evident that  $\hat{\phi}^1(\omega_x, \omega_y)$  is a low pass filter in two dimensions, hence performing the role of extracting the average of the map; on

the other hand  $|\hat{\psi}^1(\omega_x, \omega_y)|$  is a low pass filter for the x-direction and a high pass filter for the y-direction, responding to variations in the vertical direction. In a similar way  $|\hat{\psi}^2(\omega_x, \omega_y)|$  responds to variations on the horizontal direction, while  $|\hat{\psi}^3(\omega_x, \omega_y)|$  is a high pass filter both for horizontal and vertical frequencies, hence responding to variations along diagonals.

Each image is consequently decomposed following the same scheme of the multiresolution analysis into a set of blurred versions plus a set of details. The only difference is that at each level of decomposition a set of 3 matrices of details are obtained, called vertical, horizontal, and diagonal. Considering that this analysis can be performed on each field component, this results in a considerable amount of data to be analyzed.

Two main issues arise at this point: the first one comes from the previous consideration, since it is not always easy to deal with big amount of data. An efficient way to treat them is needed, and it should be characterized by a highly synthetic approach. This issue is addressed in the next section.

Furthermore, there is the need of a proper choice of the wavelet family to be used: after several different tests, the authors’ choice is to use biorthogonal wavelets, since they are symmetric and are the best choice for image processing.

## V. NUMERICAL RESULTS

### A. Data post processing

A careful analysis of the whole set of data – i.e. E field in each direction decomposed at different levels – has been performed, with the aim of determining their most significant subset and define a simple technique which is able to solve our problem.

A simple 1-level wavelet decomposition is enough to evidence the signatures of the bombs and the clutters.

Furthermore, through numerous tests, it has been observed that the most significant information is given by the z component of the electric field. Figure 5 shows the color maps relative to the magnitude of the z component of the total electric field on the observation plane of two targets, PMA

and PMN, and of the two clutters, cylindrical (#1) and spherical (#2).

The wavelet expansion of the total field on the observation plane when the soil is absent is necessary to construct a first level signature of the considered target. The signature is a crucial parameter in the discrimination of the unknown object as a target or as a simple clutter.

Figure 6 reports the diagonal coefficients of the 1-level wavelet expansion performed on the previous map of the  $E_z$ -component of a PMN mine, respectively in vacuum and buried.

Figure 7 reports the diagonal coefficient of the 1-level wavelet expansion of the  $E_z$ -component of a PMA mine. Finally, Fig. 8 reports the diagonal coefficients of the 1-level wavelet expansion of the  $E_z$ -maps of the two considered buried clutters.

In all the previous figures, brighter colors are related to higher magnitudes on a scale of 255 tones.

At first sight, it is obvious how the use of the wavelet expansion allows determining the characteristic behavior of the different objects, which is not visible by simply analyzing the electric field maps.

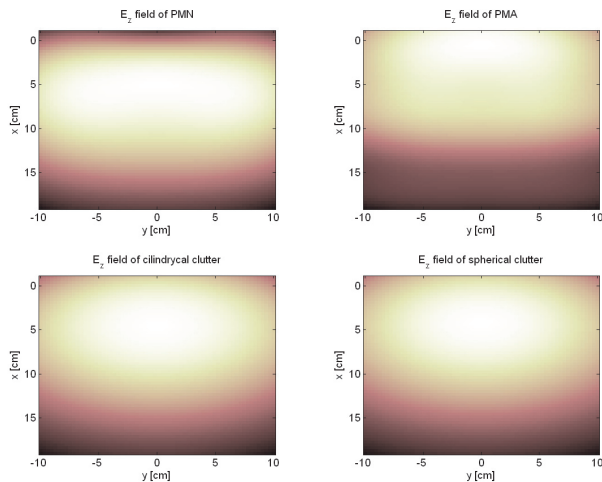
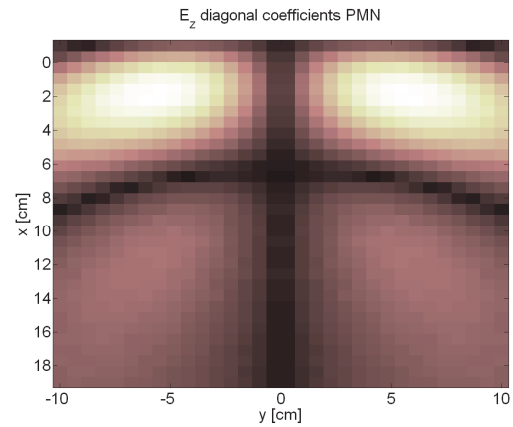
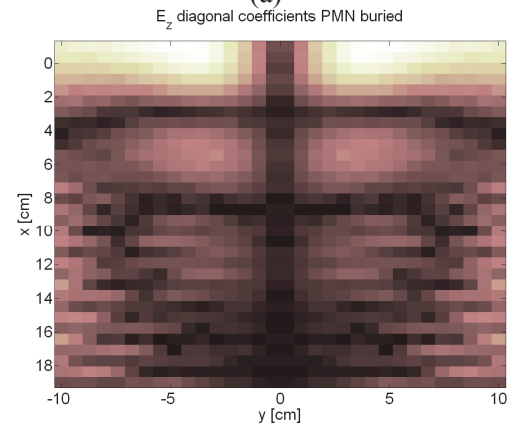


Fig. 5. z-component of the total electric field on the observation plane for the two targets and the two clutters.

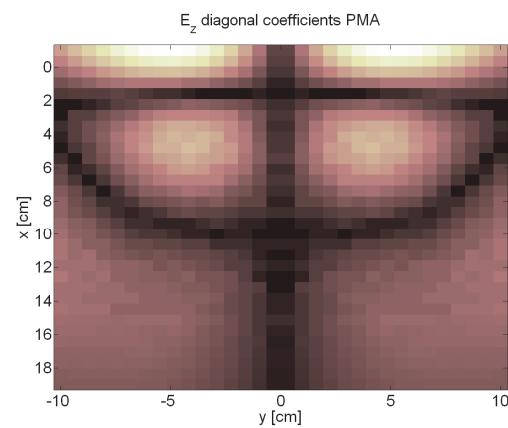


(a)

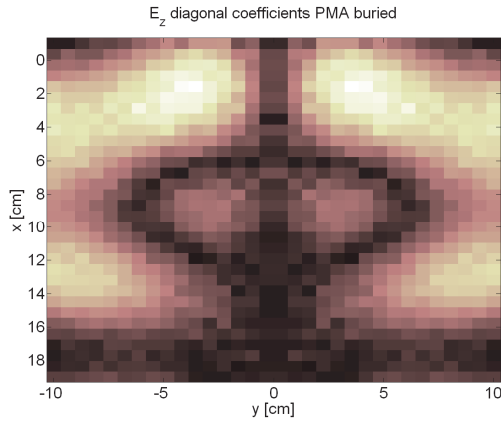


(b)

Fig. 6. Diagonal coefficients of the wavelet expansion of the  $E_z$  electric field related to the PMN bomb a) in vacuum , b) buried.

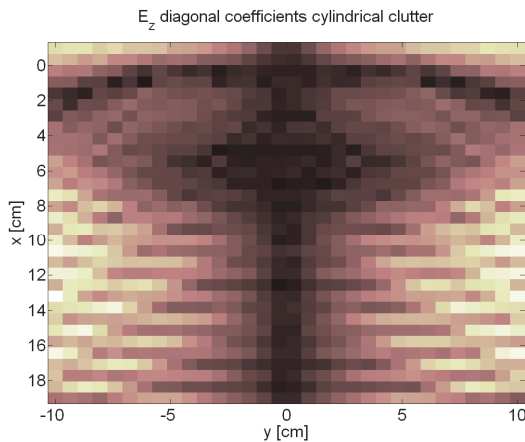


(a)

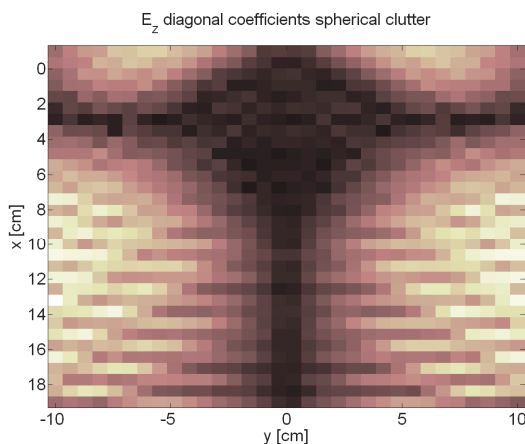


(b)

Fig. 7. Diagonal coefficients of the wavelet expansion of the  $E_z$  electric field related to the PMA bomb a) in vacuum, b) buried.



(a)



(b)

Fig. 8. Diagonal coefficients of the wavelet expansion of the  $E_z$  electric field related to a) the buried cylindrical, b) spherical clutters.

It is also easy to note how the signatures of the two clutters are very similar to each other and very different from the signatures of the bombs in empty spaces. On the other hand, the signatures of the buried bombs can be easily recognized in the figures, comparing them with the signature of the bombs in empty space.

The conclusion drawn by simply looking at the color maps of the details can also be obtained by calculating the correlation between the single maps. The correlation between two matrices yields a coefficient which gives information about how the two matrices are correlated: a higher coefficient means highly correlated matrices, while a lower coefficient substantially means two different matrices.

We start from the knowledge of the diagonal details for 4 levels of decomposition of the two bombs in free space. For each single level the correlation between the diagonal details of the unknown object and the two bombs in free space is calculated and the coefficients of all the levels of decomposition are added up to obtain a single coefficient. The results are shown in Table 1. It is worth noting that the 5-level decomposition is possible on a grid of 64 points but it is useless since it does not add any information content.

Table 1: Correlation coefficients of the unknown target (clutter or bomb) with the two bombs

	PMA	PMN
PMA buried	2.2	-3
PMN buried	-0.4	1.5
Clutter1	2.1	-2.2
Clutter2	2.2	-1.9

The grey cells show a high correlation, which means that the two bombs can be recognized, but at the same time the clutters would lead to a false alarm since they would be related to a PMA bomb. In this case, a visual analysis of the color maps is necessary to definitely discern the clutters from the real bomb.

## B. Robustness analysis

In order to take into account the typical errors present in practical measurements, a Gaussian white noise has been added to all the simulations relative to buried objects (PMA, PMN, Clutter 1 and Clutter 2), while the vacuum simulations of

the PMA and PMN have been kept as in the previous subsection.

The procedure previously explained for the calculation of the correlation has been performed again for a statistically significant set of cases. The results are reported in Table 2, which shows the probability of positive correlation.

The results are in accordance with Table 1; the same grey cells show the highest probability of positive correlations, meaning that the two bombs can be recognized, but at the same time the clutters would lead to a false alarm since they would be related to a PMA bomb. At the same time, there is a 29% percent of probability that a PMN bomb would be recognized as PMA, which is of course not an exact detection but it doesn't lead to any risky situation.

Table 2: Correlation coefficients of the unknown target (clutter or bomb) with the two bombs when noise is added

	PMA	PMN
PMA buried	0.97	0.00
PMN buried	0.29	0.90
Clutter1	0.97	0.02
Clutter2	0.97	0.05

## VI. CONCLUSION

The paper presents the numerical study of a GPR set-up for the electromagnetic detection of buried objects. The MoM method is used for the full-wave simulation of the whole set-up with targets and clutters. A post-processing based on the Wavelet decomposition of 2D electric field maps is proposed. The Wavelet decomposition makes easy the discrimination between targets and clutters but further investigations and improvements are necessary to reduce the false alarms.

## REFERENCES

- [1] I. J. Won, D. A. Keiswetter, and T. H. Bell, "Electromagnetic Induction Spectroscopy for Clearing Landmines," *IEEE Trans. Geosci. Remote Sensing*, vol. 39, no. 4, pp. 703-709, April 2001.
- [2] D. J. Daniels, *Ground Penetrating Radar 2nd Edition. IEE Radar, Sonar, Navigation and Avionics Series 15*, Institution of Electrical Engineers, London 2004.
- [3] K. P. Prokopidis, T. D. Tsiboukis, "Modeling of Ground-Penetrating Radar for Detecting Buried Objects in Dispersive Soils," *Applied Computational Electromagnetic Society (ACES) Journal*, vol. 22, no. 2, pp. 287-294, July 2007.
- [4] C. H. Huang, C. C. Chiu, C. J. Lin, and Y. F. Chen, "Inverse Scattering of Inhomogeneous Dielectric Cylinders Buried in a Slab Medium by TE Wave Illumination," *Applied Computational Electromagnetic Society (ACES) Journal*, vol. 22, no. 2, pp. 295-301, July 2007.
- [5] C. C. Chen, S. Nag, W. D. Burnside, J. I. Halman, K. A. Shubert, and L. Peters, "A Standoff Focused-Beam Land Mine Radar," *IEEE Trans. Geosci. Remote Sensing*, vol. 38, no. 1, pp. 507-514, Jan. 2000.
- [6] C. C. Chen, K. R. Rao, R. Lee, "A New Ultrawide-Bandwidth Dielectric-Rod Antenna for Ground-Penetrating Radar Applications," *IEEE Trans. Antennas Propagat.*, vol. 51, no. 3, pp. 371-377, March 2003.
- [7] P. Van Genderen, L. Nicolaescu, and J. Zijderveld, "Some Experience with the Use of Spiral Antennas for a GPR for Landmine Detection," *Proc. Int. 2003 Radar Conference*, pp. 219-223.
- [8] C. Huang, C. Chen, C. Chiu, and C. Li, "Reconstruction of the Buried Homogenous Dielectric Cylinder by FDTD and Asynchronous Particle Swarm Optimization," *Applied Computational Electromagnetic Society (ACES) Journal*, vol. 25, no. 8, pp. 672-681, August 2010.
- [9] R. Araneo and S. Celozzi, "Numerical Analysis of Subsurface Objects Discrimination Systems," *IEEE Transactions on Magnetics*, vol. 39, no. 3, pp. 1219-1222, May 2003.
- [10] S. C. Abrahams and K. Nassau, *Encyclopedia of Materials Science and Engineering*, Pergamon Press, 1986.
- [11] A. F. Peterson, S. L. Roy, and R. Mittra, *Computational Methods for Electromagnetics*, IEEE Press, Piscataway, NJ, 1997.
- [12] E. Miller, L. Medgyesi-Mitschang, and E. H. Newman, *Computational Electromagnetics*,

- Frequency-Domain Method of Moments*, Piscataway, NJ, IEEE Press, 1992.
- [13] K. A. Michalski and D. Zheng, "Electromagnetic Scattering and Radiation by Surfaces of Arbitrary Shape in Layered Media, Part I: Theory," *IEEE Trans. Antennas Propagat.*, vol. 38, no. 3, pp. 335-344, March 1990.
- [14] K. A. Michalski, J. R. Mosig, "Multilayered media Green's Functions in Integral Equation Formulations," *IEEE Trans. Antennas Propagat.*, vol. 45, no. 3, pp. 508-519, March 1997.
- [15] K. R. Aberegg, A. Taguchi, and A. F. Peterson, "Application of Higherorder Vector Basis Functions to Surface Integral Equation Formulations," *Radio Sci.*, vol. 31, no. 5, pp. 1207-1213, Sep. 1996.
- [16] R. D. Graglia, "On the Numerical Integration of the Linear Shape Functions Times the 3-D Green's Function or its Gradient on a Plane Triangle," *IEEE Trans. Antennas Propagat.*, vol. 41, no. 10, pp. 1448-1455, Oct. 1993.
- [17] D. A. Dunavant, "High Degree Efficient Symmetrical Gaussian Quadrature Rules for the Triangle," *Intern. J. Num. Meth. Engin.*, vol. 21, pp. 1129-1148, Jun. 1985.
- [18] K. A. Michalski, "Extrapolation Methods for Sommerfeld Integral Tails," *IEEE Trans. Antennas Propagat.*, vol. 46, no. 10, pp. 1405-1418, Oct. 1998.
- [19] C. Bruns, P. Leuchtman, and R. Vahldieck, "Analysis and Simulation of a 1-18 GHz Broadband Double-Ridged Horn Antenna," *IEEE Trans. Electromagn. Compatibil.*, vol. 45, no. 1, pp. 55-60, Feb. 2003.
- [20] Z. Zhang and R. E. Diaz, "Simulation of Broadband Double-Ridged Horn in High-Fidelity Material Characterization using Finite-Difference Time-Domain Method," *2005 IEEE Antennas and Propagation Society Int. Symp.*, vol. 1B, pp. 561-564.
- [21] MIMÉVA: Study of generic Mine-like Objects for R&D in Systems for Humanitarian Demining, <http://humanitarian-security.jrc.it/>.
- [22] S. G. Mallat, *A Wavelet Tour of Signal Processing*, Academic Press.
- [23] W. Chen, X. Yang, and Z. Wang, "Application of Wavelets and Auto-Correlation-Function For Cancellation of High-Frequency EMI Noise," *Applied Computational Electromagnetic Society (ACES) Journal*, vol. 24, no. 3, pp. 332-336, June 2009.
- [24] S. Barmada, A. Landi, M. Papi, and L. Sani, "Wavelet Multi-Resolution Analysis for Monitoring the Occurrence of Arcing on Overhead Electrified Railways," *Proc. Instn Mech. Engrs*, vol. 217, part. F: J. Rail and Rapid Transit, pp. 177-187.
- [25] S. Perrin, A. Bibaut, E. Duflos, and P. Vanheeghe, "Use of Wavelets for Ground-Penetrating Radar Signal Analysis and Multisensor Fusion in the Frame of Land Mine Detection," *2000 IEEE International Conference on Systems, Man, and Cybernetics*, vol. 4, pp. 2940-2945.



**Rodolfo Araneo** was born in Rome, Italy, on October 29, 1975. He received the M.S. (cum laude) and Ph.D. degrees in Electrical Engineering from the University of Rome "La Sapienza", Rome, in 1999 and 2002, respectively.

During the master thesis in 1999, he was a Visiting Student at the National Institute of Standards and Technology (NIST) Boulder, CO where he worked on TEM cells and shielding. During the second semester of the year 2000, he was a Visiting Researcher of the Department of Electrical and Computer Engineering of University of Missouri-Rolla (UMR) where he worked on printed circuit boards and finite difference time-domain techniques.

Dr. Araneo received the Past President's Memorial Awards in 1999 from IEEE EMC Society. His research activity is mainly in the field of electromagnetic compatibility (EMC) and includes numerical and analytical techniques for modeling high-speed printed circuit boards, shielding, and transmission line analysis.



**Sami Barmada** was born in Livorno, Italy, in 1970. He received the Master (cum laude) and Ph.D. degrees in Electrical Engineering from the University of Pisa, Italy, in 1995 and 2001, respectively.

From 1995 to 1997, he was with ABB Teknologi, Oslo, Norway, where he was involved with distribution network analysis and optimization. He is currently an Associate Professor with the Department of Energy and Systems Engineering, University of Pisa, where he is involved with numerical computation of electromagnetic fields, modeling of multiconductor transmission lines, powerline communications.

He is author of about 100 papers published on international journals and peer reviewed conference proceedings.

Prof. Barmada was the technical chairman of the Progress in Electromagnetic Research Symposium (PIERS), Pisa, Italy, 2004 and the general chairman of the ACES 2007 conference in Verona, Italy.

He was the recipient of the 2003 J F Alcock Memorial Prize, presented by The Institution of Mechanical Engineering, Railway Division, for the best paper in technical innovation and he currently is IEEE Senior Member and ACES member.